Figure 1.

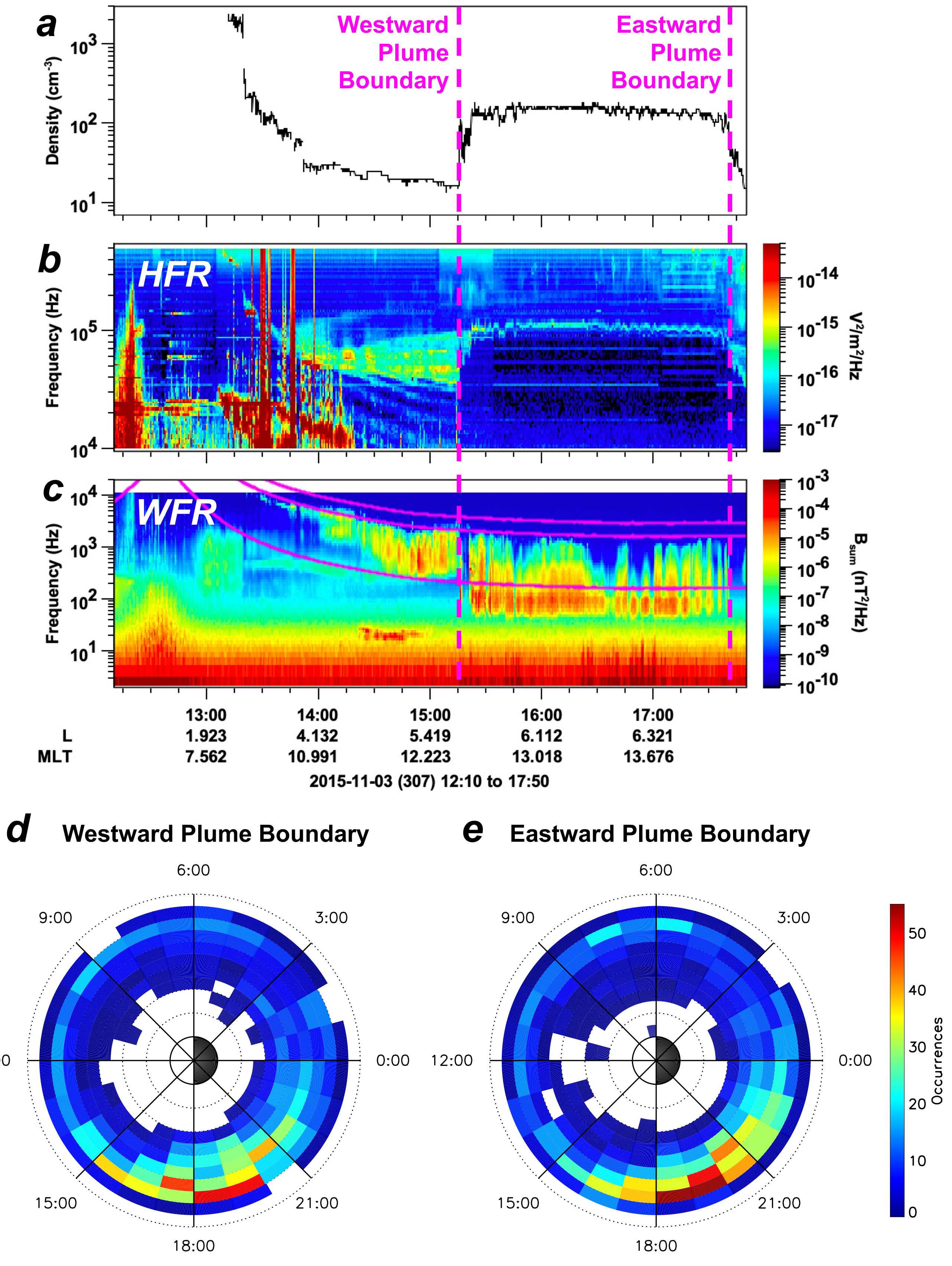

a
Density (cm-3)
Westward Plume Boundary
Eastward Plume Boundary
b
HFR
Frequency (Hz)
V²/m²/Hz
c
WFR
Frequency (Hz)
Bsum (nT²/Hz)
13:00 14:00 15:00 16:00 17:00
L 1.923 4.132 5.419 6.112 6.321
MLT 7.562 10.991 12.223 13.018 13.676
2015-11-03 (307) 12:10 to 17:50
d
Westward Plume Boundary
e
Eastward Plume Boundary
6:00
3:00
9:00
12:00
0:00
15:00
21:00
18:00
Occurrences

Figure 2.

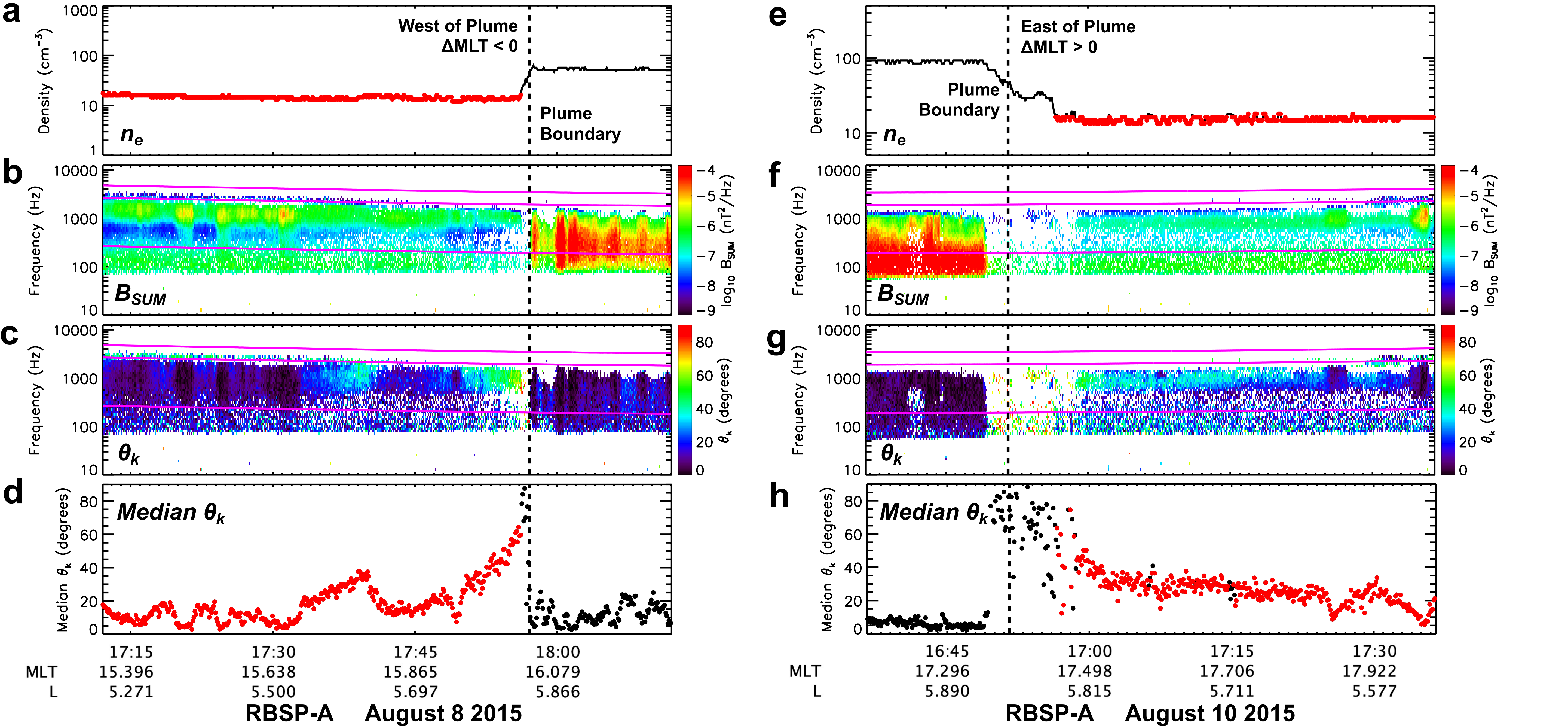

a
West of Plume
ΔMLT < 0
Plume
Boundary
Density (cm⁻³)
n_e
b
Frequency (Hz)
B_SUM
log10 B_SUM (nT²/Hz)
c
θ_k
θ_k (degrees)
d
Median θ_k
Median θ_k (degrees)
17:15
17:30
17:45
18:00
MLT
15.396
15.638
15.865
16.079
L
5.271
5.500
5.697
5.866
RBSP-A August 8 2015
e
East of Plume
ΔMLT > 0
Plume
Boundary
f
g
h
16:45
17:00
17:15
17:30
17.296
17.498
17.706
17.922
5.890
5.815
5.711
5.577
RBSP-A August 10 2015

Figure 3.

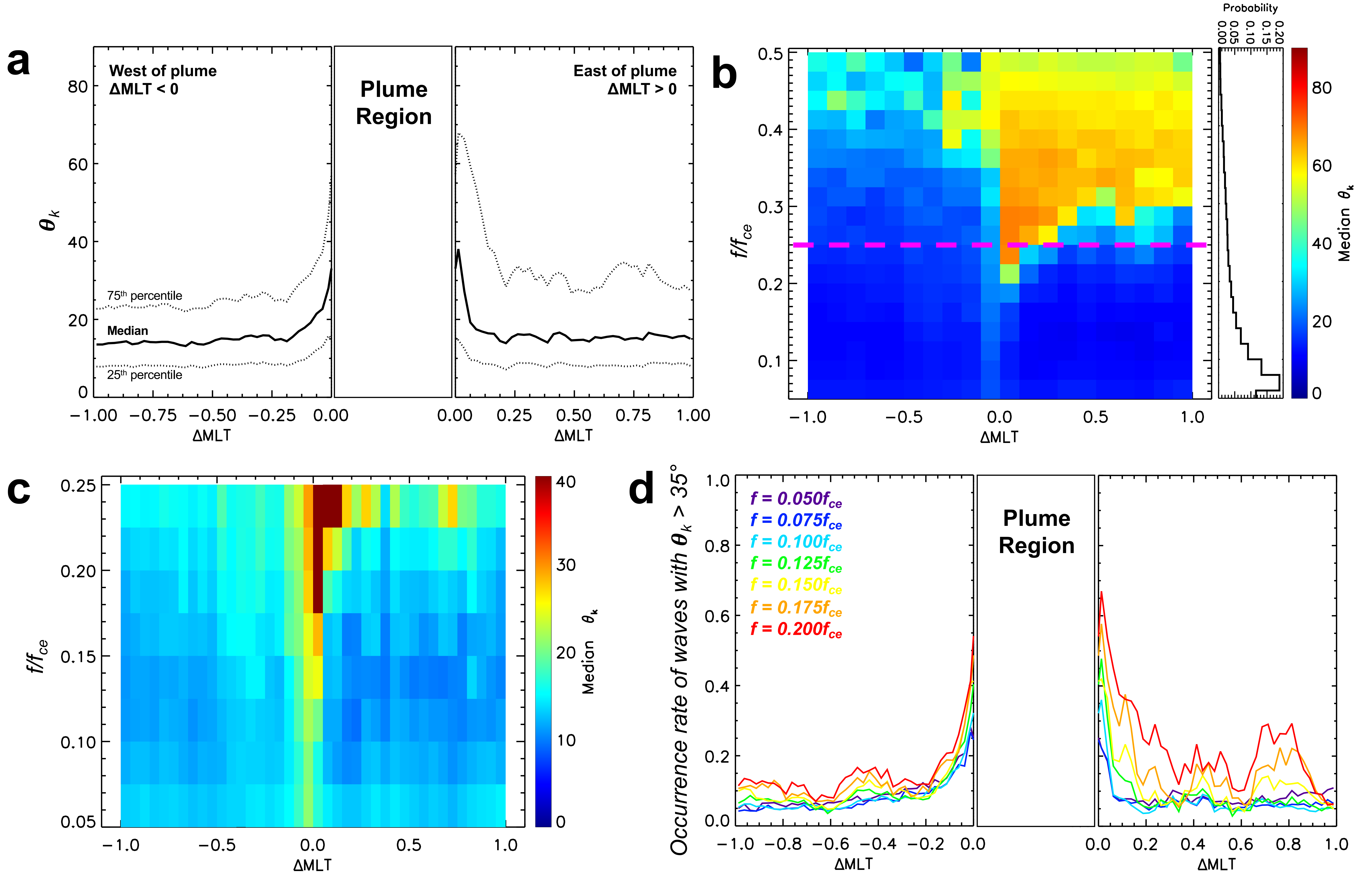

a
West of plume
ΔMLT < 0
Plume Region
East of plume
ΔMLT > 0
75th percentile
Median
25th percentile
θk
ΔMLT
b
f/fce
ΔMLT
Probability
Median θk
c
f/fce
ΔMLT
Median θk
d
Occurrence rate of waves with θk > 35°
f = 0.050fce
f = 0.075fce
f = 0.100fce
f = 0.125fce
f = 0.150fce
f = 0.175fce
f = 0.200fce
Plume Region
ΔMLT

Figure 4.

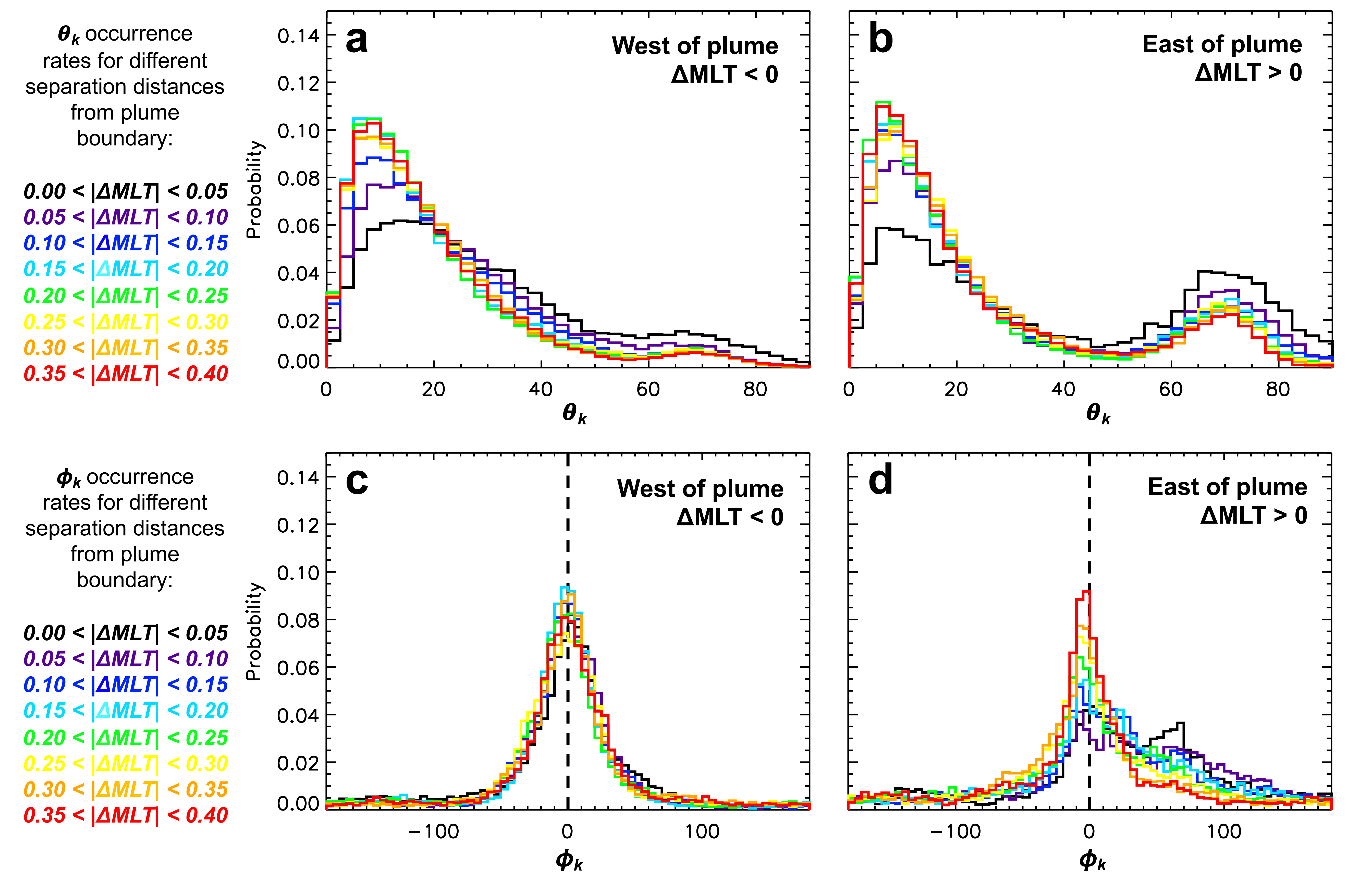
θk occurrence rates for different separation distances from plume boundary:
0.00 < |ΔMLT| < 0.05
0.05 < |ΔMLT| < 0.10
0.10 < |ΔMLT| < 0.15
0.15 < |ΔMLT| < 0.20
0.20 < |ΔMLT| < 0.25
0.25 < |ΔMLT| < 0.30
0.30 < |ΔMLT| < 0.35
0.35 < |ΔMLT| < 0.40
a
West of plume
ΔMLT < 0
b
East of plume
ΔMLT > 0
Probability
θk
φk occurrence rates for different separation distances from plume boundary:
0.00 < |ΔMLT| < 0.05
0.05 < |ΔMLT| < 0.10
0.10 < |ΔMLT| < 0.15
0.15 < |ΔMLT| < 0.20
0.20 < |ΔMLT| < 0.25
0.25 < |ΔMLT| < 0.30
0.30 < |ΔMLT| < 0.35
0.35 < |ΔMLT| < 0.40
c
West of plume
ΔMLT < 0
d
East of plume
ΔMLT > 0
Probability
φk

The Angular Distribution of Lower Band Chorus Waves Near Plasmaspheric Plumes

D. P. Hartley[1], L. Chen[2], I. W. Christopher[1], C. A. Kletzing[1], O. Santolik[3, 4],

W. Li[5], R. Shi[6]

[1]Department of Physics and Astronomy,

University of Iowa, Iowa City, Iowa, USA.

[2]University of Texas at Dallas,

Richardson, Texas, USA.

[3]Department of Space Physics, Institute

of Atmospheric Physics, Prague, Czech

Republic.

[4]Faculty of Mathematics and Physics,

Charles University, Prague, Czech Republic.

[5]Center for Space Physics, Boston

University, Boston, USA.

[6]Tongji University, Shanghai, China.

Plumes have been identified as an access region for chorus waves to enter the plasmasphere. Here, for the first time, chorus wave properties are parameterized by distance from the plume boundary. Case studies and statistical analysis indicate that the polar wave vector angle, θ_k, of chorus becomes more oblique near the plume edge. Occurrence rates of $\theta_k > 35°$ on the plume boundary are approximately double that observed further away from the plume. Whilst the increase in θ_k is apparent on both plume edges, the distribution of θ_k exhibits different behavior between the Eastward and Westward boundaries. In general, the distribution of azimuthal wave vector angles, ϕ_k, is symmetric about the anti-Earthwards direction. However, near the Eastward plume boundary, an Eastwards skew of ϕ_k is reported. This result provides new insight on chorus propagation in the context of the chorus-to-hiss mechanism, and has implications for quantifying wave-particle interactions in the near-plume region.

1. Introduction

Whistler-mode chorus waves are naturally occurring electromagnetic emissions that can be observed as short bursts with rising or falling tone elements, but may also be observed as a hiss-like emission [*Pope*, 1963; *Cornilleau-Wehrlin et al.*, 1978; *Koons*, 1981; *Santolík et al.*, 2009; *Li et al.*, 2012]. The frequency range for chorus waves scales with the equatorial electron cyclotron frequency, f_{ce} (e.g. *Gurnett and O'Brien*, 1964; *Xiao et al.*, 2017). The maximum frequency is around 0.90 f_{ce} and the typical lower limit near 0.05 f_{ce}, although lower frequency chorus waves down to the lower hybrid resonance frequency have also been observed (e.g. *Meredith et al.*, 2014; *Cattell et al.*, 2015; *Gao et al.*, 2016). Chorus may be observed with a spectral gap located near 0.50 f_{ce}, with waves below (above) this gap called lower (upper) band chorus (e.g. *Burtis and Helliwell*, 1969; *Tsurutani and Smith*, 1974; *Koons and Roeder*, 1990; *Li et al.*, 2019; *Teng et al.*, 2019; *Gao et al.*, 2019). Typically, lower band chorus waves are more intense than upper band chorus (e.g. *Meredith et al.* [2020]) which can drive strong pitch-angle and energy diffusion of electrons in the radiation belts (e.g. *Horne et al.* [2013]; *Allison et al.* [2021]).

It has been shown that chorus waves in the lower half of the lower band chorus wave frequency band can propagate in such a way that they enter the plasmasphere, and may provide a source of plasmaspheric hiss. Multi-spacecraft measurements have shown a correlation between the power of chorus waves and plasmaspheric hiss observed with a small delay [*Bortnik et al.*, 2009; *Wang et al.*, 2011; *Li et al.*, 2015]. The Time History of Events and Macroscale Interactions during Substorms (THEMIS) mission was used by *Agapitov et al.* [2018] to show a statistical correlation between chorus and hiss, with the correlation occurring most frequently in the post-noon sector. *Hartley et al.* [2019] showed that plasmaspheric plumes may be the reason for the high correlations occurring in this region, and identified plumes as providing an access region for chorus to enter the plasmasphere. Ray tracing simulations show that in the typical case, the chorus wave vector is required to be both oblique and oriented towards the Earth for the wave to propagate into the plasmasphere (e.g. *Chum and Santolík*, 2005; *Santolík et al.*, 2006; *Bortnik et al.*, 2008, 2011a, b, 2016; *Zhou et al.*, 2016; *Hartley et al.*, 2018). However, the range of wave vector orientations that can access the plasmasphere becomes significantly larger for chorus sources located right on the edge of plasmaspheric plumes in comparison to chorus at other source locations (e.g. *Chen et al.*, 2009; *Hartley et al.*, 2019).

In previous studies, the characteristics of chorus waves have been parameterized spatially as a function of L (or L*) and MLT (e.g. *Meredith et al.*, 2003, 2011, 2021; *Li et al.*, 2015). Several studies have also investigated the properties of whistler-mode waves inside of plasmaspheric plumes (e.g. *Kim and Shprits*, 2019; *Shi et al.*, 2019). Here, for the first time, we specifically study chorus wave vector characteristics in the vicinity of plasmaspheric plumes, parameterizing observations by distance from the plume boundary. The importance of sorting wave properties by density boundaries has previously been demonstrated for both chorus waves [*Malaspina et al.*, 2021] and plasmaspheric hiss [*Malaspina et al.*, 2016]. As such, this analysis provides a more natural characterization of chorus wave properties near plumes in the context of the chorus-to-hiss mechanism.

2. Plume and Chorus Identification using EMFISIS Observations

The Van Allen Probes [*Mauk et al.*, 2012] EMFISIS Waves instrument [*Kletzing et al.*, 2013] captures 500 ms waveforms of both the magnetic and electric field every 6 seconds. These waveforms are used to calculate six-dimensional spectral matrices onboard the spacecraft. The singular value decomposition (SVD) method is subsequently used to calculate wave propagation characteristics once data have been sent to the ground [*Santolík et al.*, 2003b]. The plasma density is inferred from the upper hybrid resonance frequency as described in *Kurth et al.* [2015].

For each half-orbit, the plasma density, electric field wave observations between 10 kHz and 400 kHz (HFR), and electric and magnetic wave observations between 2 Hz and 12 kHz (WFR) are plotted. From these plots, density enhancements are manually identified. An advantage of manual identification is that we can recognize density enhancements that span spacecraft apogee which may have been disregarded in some autonomous identification methods. A downside is that manual identification is somewhat subjective, and may not adhere to a quantitative definition. Note that here, multiple density enhancements may be identified in a single half-orbit. Of these density enhancements, any that exceed 0.2 Earth radii in either the radial or azimuthal direction are considered to be plasmaspheric plumes. Across the entire Van Allen Probes mission, 1,740 plumes have been identified using data from both spacecraft, with the East and West plume boundaries stored for further analysis

Figure 1 shows an example of (a) the plasma density, (b) the HFR electric field data, and (c) the WFR magnetic field wave data during a plasmaspheric plume observation in the RBSP-B data on November 3, 2015. The Westward and Eastward plume boundaries are indicated by dashed pink lines. Chorus activity is apparent in the WFR data prior to the observation of the Westward plume boundary. Figure 1 further shows statistics of the locations of the (d) Westward and (e) Eastward plume boundaries in L (radial axis) and MLT (azimuthal direction). These distributions indicate that plumes most commonly occur on the duskside, and occasionally near the dawnside, consistent with previous work (e.g. *Darrouzet et al.*, 2008; *Usanova et al.*, 2013; *Kim and Shprits*, 2019).

Having identified a list of plasmaspheric plumes, the next step is to identify chorus waves that occur in close proximity. Similar to previous studies (eg. *Li et al.* [2014]; *Hartley et al.* [2015, 2016, 2019]; *Bingham et al.* [2018]), waves are categorized as chorus if they meet the following criteria.

1. Wave power exceeds 10^{-9} nT^2/Hz or 5 $\times$ the instrument background levels, whichever is higher.

2. Planarity [*Santolík et al.*, 2003b], ellipticity [*Santolík et al.*, 2002], and 2D degree of coherence in the polarization plane [*Santolík and Gurnett*, 2002] all exceed 0.5.

3. Plasma density is less than $10\times(6.6/\mathrm{L})^4$ or 30 cm^{-3}, whichever is smaller.

4. Plasma density is at least a factor of 1.5 below the average density of the nearest plume.

Instrument background levels are listed at http://emfisis.physics.uiowa.edu/Events/rbsp-a/backgrounds/ and http://emfisis.physics.uiowa.edu/Events/rbsp-b/backgrounds/. Criterion 1 ensures sufficient signal in the wave observations. Criterion 2 ensures that no more than 14% of the total wave power, or 25% of power with respect to the largest axis of the 3-D polarization ellipsoid, is outside of the polarization plane [*Hartley et al.*, 2018] and that the wave normal direction determined using SVD (which assumes the presence of a plane wave) [*Santolík et al.*, 2003b] is well-defined. Criterion 3 is used to ensure that the spacecraft are outside of the plasmasphere, in the low-density plasmatrough region. Criterion 4 is implemented to limit the inclusion of data from inside any plume-adjacent density enhancements, as well as to ensure the plume density is a factor of 1.5, or greater, above the density at the time of the chorus observation (indicating a density gradient is present).

The criteria listed above ensure that all waves included in this analysis are coherent, right-handed, near circularly polarized, and located outside of the plasmasphere, as would be expected for whistler-mode chorus waves.

Having identified chorus waves that occur close to the boundaries of plasmaspheric plumes, it is now possible to investigate the angular distribution of these waves both for individual case study events, and statistically, as described in the following sections.

3. Case Studies of Chorus Near Plumes

Two case study events are investigated where chorus waves are observed near plumes. Figure 2 shows (a and e) the plasma density, n_e, (b and f) the total magnetic field wave power, B_{SUM}, (c and g) the polar wave vector angle, θ_k, and (d and h) the median θ_k in the lower band chorus wave frequency range (0.05 to 0.50 f_{ce}). Here, θ_k is defined as the angle between the background magnetic field and the wave vector, k. Overplotted magenta lines indicate 0.05, 0.50 and 0.90 f_{ce} whereas the vertical black dashed lines indicate the plume boundaries. Data are only shown in panels b, c, f, and g if criteria 1 and 2, defined in Section 2, are met. Data are indicated by red dots in panels a, d, e, and h if density observations meet criteria 3 and 4, and black dots if they do not.

For the first case study event (left), a Westward plume boundary is observed at 17:57 on August 8 2015 by RBSP-A. As the spacecraft is West of the plume boundary, lower band chorus waves are observed between 0.05 and 0.50 f_{ce}. Towards the start of the plotted interval, these waves propagate approximately parallel to the background magnetic field with small θ_k. The median wave normal angle of lower band chorus during this time is less than 20°. Around 17:32 a change in θ_k is observed, with values starting to increase as the spacecraft gets closer to the plasmaspheric plume density structure. The median wave normal angle increases to above 20° at this time. The median wave normal angle then decreases somewhat to a local minima near 17:45, before increasing drastically to over 50° directly on the plume edge at 17:57. This behavior is also apparent in Figure 2c close to the plume edge. This is the first indication that chorus waves are observed to propagate with increasing obliquity near the plume boundary.

For the second case study event (right), an Eastward plume boundary is observed by RBSP-A at 16:52 on August 10 2015. We note in this event that data are not included in the analysis directly on the plume edge as the plasma density exceeds the implemented thresholds. So while the plume edge is observed at 16:52, data are not included in this analysis until 16:56, as indicated by the red data points in Figure 2e and h. Near 17:00, close to the plume edge, lower band chorus waves are observed between 0.05 and 0.50 f_{ce}. The wave normal angle at this time is close to, or greater than, 40°. As the spacecraft moves further away from the plume edge, a decrease in the wave normal angle is observed, with the median wave normal angle being closer to 20°. Again, similar to the first case study event, the wave normal angle is observed to be more oblique near the plume boundary when compared to larger separation distances from the plume.

From investigating the wave normal angle of lower band chorus waves during these two case study events we have shown the following two features. First, at large separation distances from the plume boundary, chorus waves are primarily observed with small θ_k and are approximately field-aligned. Second, near the edge of the plume boundary, θ_k becomes more oblique, with this behavior observed on both a Westward (Case Study 1) and an Eastward (Case Study 2) plume edge. Investigation of further case study events reveals that this signature in θ_k is apparent in multiple observations of chorus waves that occur near plume boundaries. This feature is demonstrated in the following statistical analysis.

4. Statistical Analysis of Chorus Near Plumes

Chorus wave observations near all 1,740 plumes identified in the data of both Van Allen probes are binned as a function of separation distance from the plume boundary both in magnetic local time (MLT) and L shell. Here, due to the spacecraft trajectory, we consider statistics of the wave normal angle as a function of separation distance from the plume in MLT. This is due to most plumes being observed close to spacecraft apogee (see Figure 1d and e), where motion is primarily in the azimuthal direction (i.e. in MLT, rather than L).

Figure 3a shows the median wave normal angle of lower band chorus waves sorted by separation distance from the plume in MLT. The 25th and 75th percentiles are also shown by dotted lines. Note that here, data are accumulated by individually counting each time interval and instrument frequency channel where chorus is observed, before being binned by each ΔMLT interval. The median value, and the percentiles, are then calculated using θ_k values obtained for all these times and frequencies.

West of the plume boundary (ΔMLT < 0), the median wave normal angle remains approximately constant near 15° for separation distances greater 0.2 MLT away from the plume, while the 25th percentile and 75th percentile remain near 8° and 25°, respectively. For data closer than 0.2 MLT to the plume boundary, the median, 25th, and 75th percentiles begin to increase up to a maximum value that occurs right at the plume edge. Directly on the boundary, the median wave normal angle is near 35°, and the 25th and 75th percentiles are approximately 15° and 55°, respectively.

East of the plume boundary (ΔMLT > 0) presents a somewhat similar picture, although there is a larger degree of variation in the median wave normal angle overall due, in part, to less abundant chorus waves in this MLT region. However, the median wave normal angle is again relatively constant around 15° for separation distances larger than 0.2 MLT. For closer separation distances, the median wave normal angle increases up to maximum value near 40° on the plume edge.

From Figure 3a it is apparent that the median wave normal angle, as well as the 25th and 75th percentiles, increase near the plume edges. This indicates that the behavior of chorus waves becoming more oblique in the near-plume-edge region that was demonstrated for individual case study events in Figure 2, is also apparent in the statistical sense.

For the statistical analysis presented so far, the wave normal direction has been averaged over the entire lower band chorus frequency range. Here, we now consider the frequency dependence.

Figure 3b and c show the median wave normal angle of lower band chorus as a function of wave frequency normalized to the equatorial electron cyclotron frequency and separation distance from the plume in MLT for (b) all frequencies and (c) frequencies below f/f_{ce} < 0.25. The probability distribution as a function of wave frequency is also shown. Note that the color bar for panel (b) is between 0° and 90 °, whereas the color bar for panel (c) is between 0° and 40°. The magneta line on Figure 3b indicates $f/f_{ce} = 0.25$. The reduction in the range of θ_k values shown in Figure 3c is to highlight that the increase in θ_k is apparent all the way down to 0.05 f_{ce}, although the magnitude of the increase is somewhat less for lower frequencies. This low frequency range is also where most of the observations occur, as shown by the probability distribution.

The median wave normal angle indicates that oblique chorus waves are generally more apparent East of the plume (ΔMLT > 0), particularly above $f/f_{ce} = 0.25$. This is likely a coincident feature due, in part, to the MLT range where plumes are observed as shown in Figure 1. *Li et al.* [2016] showed that chorus waves with $\theta_k > 40°$ are more commonly observed between 19:00 and 09:00 in MLT, and as such, this may be an MLT dependent feature, rather than a feature associated with the plume itself. However, in Figure 3c we focus on normalized wave frequencies below $f/f_{ce} = 0.25$, which has been shown to be the important frequency range for the chorus-to-hiss mechanism, and are more commonly observed as indicated by the probability distribution provided in panel b. This reveals a modest increase in θ_k apparent right on the edge of the plume boundary (ΔMLT near 0) on both the Eastward and Westward edges for all wave frequencies down to 0.05 f_{ce}. This increase extends about 0.20 MLT away from the plume boundary in both the Eastwards and Westwards direction. Given that this feature is only apparent close to the plume boundary, we attribute this characteristic directly to the presence of the plume.

To quantify the extent of the increase in oblique waves near the plume boundary, we consider the fraction of observations which exceed a specific wave normal angle value. Figure 3d shows the fraction of waves where the polar wave vector angle exceeds 35° as a function of separation distance from the plume in MLT. Different frequencies are indicated by different colors.

Far away from the plume boundary, ΔMLT > 0.5, around 10% or less of waves are observed with $\theta_k > 35°$ for most of the plotted frequencies. It is apparent that on the edge of plume structures (ΔMLT < 0.2), the occurrence of waves with $\theta_k > 35°$ increases, and the occurrence rate directly on the plume boundary is a factor of two, or more, greater than that observed further away from the plume for all of the plotted frequencies.

One possible explanation for the increase in more oblique waves is that as the chorus waves propagate from the low-density plasmatrough region, they refract near the edge of the higher density plume. These density structures have gradients perpendicular to the background magnetic field, with higher densities implying a larger refractive index. Snell's law tells us that the wave vector would incline towards the direction of the gradient in the refractive index, meaning closer to a direction perpendicular to the background magnetic field, resulting in a larger θ_k.

To summarize, a statistical investigation of the wave normal angle of lower band chorus waves near plasmaspheric plume structures has revealed that:

1. Away from the plume boundary, chorus waves are typically close to field-aligned, with small θ_k.

2. Directly on the edge of the plume boundary ($|\Delta\text{MLT}| < 0.2$) θ_k becomes more oblique.

3. This behavior is observed on both plume edges, Eastward and Westward.

5. Comparison between Eastward and Westwards Plume Boundary

The angular distribution of wave vectors near these plume boundaries is now investigated in closer detail.

Figure 4 shows probability distribution functions (PDFs) of the polar wave vector angle, θ_k, near the (a) Westward, and (b) Eastward plume boundary. Each color indicates a different range of distances from the plume in MLT, from closest to the plume in black, to furthest away from the plume in red.

West of the plume all distributions contain a large peak of near-field-aligned waves with small θ_k values, a noticeable tail towards more oblique wave normal angles, and a small secondary peak with large θ_k. It is apparent that for $|\Delta\text{MLT}| > 0.20$, all of the distributions sit on top of each other and are indistinguishable with the primary peak centered between 5° and 10°. As we move closer towards the plume, the entire PDF begins to skew towards larger θ_k values. The main distribution peak both shrinks in size, and shifts towards larger wave normal angles, with a peak centered between 15° and 20°

on the plume boundary. The maximum skew towards more oblique waves is observed for measurements directly on the plume boundary.

East of the plume all distributions exhibit a double-peaked structure with a field-aligned population with a peak located near 10° and a smaller, more oblique population with a peak located near 70°. Again, for $|\Delta \text{MLT}| > 0.20$, the distributions are almost identical. For smaller $|\Delta \text{MLT}|$ values, as we get closer to the plume, an increase in relative occurrences of the more oblique population is observed as well as a decrease in relative occurrences of the field-aligned population. However, it should be noted that the peaks of the distributions do not shift in θ_k, which is in contrast to what is observed for chorus west of the plume. The oblique population of waves appears to be most prevalent for observations directly on the plume boundary, and is actually comparable in occurrences to the field-aligned population of waves. So while the increase in median θ_k values is apparent on both the Eastward and Westward plume boundaries as shown in Figure 3, the cause of this increase is due to different variations in the distribution of θ_k.

Thus far, only the polar wave vector angle, θ_k, has been considered. We may also consider the azimuthal wave vector angle, ϕ_k, defined as the angle, with respect to the anti-Earthwards direction, of the wave vector, k. With this definition, $\phi_k = 0°$ (180°) corresponds to radially outwards from (towards) the Earth, whereas $\phi_k = 90°$ (-90°) corresponds to the Eastward (Westward) direction. Figure 4c and d show ϕ_k in the same format as used for θ_k in panels a and b. Data are only included if θ_k exceeds 30°, as this allows for a well-defined azimuthal direction.

We note that an ambiguity exists in the direction of the wave vector when considering only the magnetic field. That is, it is not possible to distinguish between cases where k has a component parallel to the background magnetic field from cases where k has a component anti-parallel to the background magnetic field. As such, spectral estimates of the polar angle of the Poynting vector, θ_S, [*Santolík et al.*,, 2010] are required to remove this ambiguity. For $\theta_S < 90°$, k is defined by ϕ_k, whereas for $\theta_S > 90°$, k is defined by $\phi_k + 180°$. This adjustment in ϕ_k for cases where $\theta_S > 90°$ has been applied to all data presented here, such that $\phi_k = 0°$ indicates the anti-Earthwards direction in all cases. Sheath impedance effects associated with electric field observations (e.g. *Hartley et al.*, 2015, 2016, 2017) are corrected for using the sheath-corrected L4 dataset described in *Hartley et al.* [2022].

West of the plume, the distribution of ϕ_k is strongly peaked around the anti-Earthwards direction ($\phi_k = 0°$) and approximately symmetric for all ΔMLT values with only minor variations. This is consistent with the statistics of chorus waves presented in *Hartley et al.* [2019], who reported that for the vast majority of occurrences, around 85%, the wave vector was oriented with a component in the anti-Earthwards direction. East of the plume, for $|\Delta\text{MLT}| > 0.20$, the distributions are approximately symmetric and centered on the anti-Earthward direction, which is consistent with ray tracing results in the meridian plane when azimuthal density gradients are weak (e.g. *Chen et al.*, 2009; *Hartley et al.*, 2019). Closer to the plume boundary however, for smaller $|\Delta\text{MLT}|$ values, the distribution of ϕ_k becomes skewed towards positive values (i.e. Eastwards). This is apparent in the increase in the distribution between 30° and 130° in Figure 4d. This change in the distribution indicates a preferential shift in the Eastwards direction of the azimuthal wave vector angle. This Eastwards shift is more apparent for $\theta_k > \theta_G$, where θ_G is the Gendrin angle [*Gendrin*, 1961]. Figure showing the distribution of ϕ_k for $30° < \theta_k < \theta_G$ and $\theta_k > \theta_G$ is provided in supporting information.

The differences in the angular distribution of lower band chorus waves between the Eastward and Westward plume boundaries may be summarized as:

1. West of plume boundary the distribution of θ_k contains a primary peak of approximately field-aligned waves and a small secondary peak with large θ_k. The primary peak skews towards more oblique waves for observations closer to the plume edge.

2. East of plume boundary the distribution of θ_k contains two peaks, a field-aligned population and a more oblique population. As the spacecraft gets closer to the plume edge, an increase in the oblique population is observed along with a decrease in the field-aligned population.

3. The azimuthal wave vector angle, ϕ_k, West of the plume is symmetric and oriented anti-Earthwards. Close to the Eastward edge of the plume boundary a skew of ϕ_k towards the Eastward direction is observed.

6. Summary and Conclusions

Plasmaspheric plumes have been shown to provide an access region for chorus waves to propagate into the plasmasphere, indicating the need to directly investigate chorus properties in the vicinity of plume structures. Here, a list of plumes has been manually identified using data from the Van Allen Probes mission, yielding a list of 1,740 events.

Case study events analyzing the wave vector orientation in the vicinity of plumes indicates that the polar wave vector angle, θ_k, becomes more oblique near the plume boundary. This increase in obliquity is observed both on the Eastward and Westward plume edges.

A statistical analysis of chorus near plumes shows that more oblique waves are typically observed within $|\Delta\text{MLT}| < 0.20$ of a plume boundary, and that the occurrence rate of more oblique waves ($\theta_k > 35°$) in this region is a factor of two, or greater, than that observed further away from the plume.

Whilst the increase in occurrences of oblique waves is apparent on both plume edges, the distribution of θ_k shows distinct differences between the Eastward and Westward boundaries. On the Westward edge, the entire θ_k distribution skews towards larger values. In contrast, on the Eastward boundary we observe an increase in the oblique population of waves and a decrease in the field-aligned population. Directly on the plume edge, these two populations are comparable.

The azimuthal wave vector angle, ϕ_k, also shows differences between the Eastward and Westward boundaries. On the Westward edge, the ϕ_k distribution is strongly peaked in the anti-Earthwards direction and symmetric. However, on the Eastward boundary, the ϕ_k distribution becomes asymmetric, with a skew towards the Eastward direction. This asymmetry is probably explained by propagation effects, likely linked to the different directions of the density gradients on the two sides of the plume.

These results provide new insight into how chorus waves propagate near plasmaspheric plumes which can be tested against ray-tracing simulations in order to better understand the chorus-to-hiss mechanism. This is planned for a future study. These results are also important for accurate quantification of wave-particle interactions in the near-plume region, which critically depends on the wave normal angle.

Acknowledgments. DPH and LC acknowledge that this material is based upon work supported by the National Aeronautics and Space Administration under Grant No. 80NSSC20K1324 issued through the Heliophysics Supporting Research Program. DPH and IWC acknowledge NASA grant 80NSSC21K0519. OS acknowledges funding from the European Union's Horizon 2020 research and innovation programme under grant agreement No. 870452 and acknowledge support from MSMT grant LTAUSA17070. WL acknowledges the NSF grant AGS-184818 and NASA grants 80NSSC20K0698 and 80NSSC19K0845.

7. Open Research

All data used during this analysis is freely available and may be obtained from http://emfisis.physics.uiowa.edu/data/index. List of plume events used in this study are available for use at http://iro.uiowa.edu/esploro/outputs/dataset/List-of-Plasmaspheric-Plumes-from-Van/9984240534702771 (DOI: 10.25820/data.006173).

References

Agapitov, O., Mourenas, D., Artemyev, A., Mozer, F. S., Bonnell, J. W., Angelopoulos, V., Shastun, V., and Krasnoselskikh, V. (2018). Spatial extent and temporal correlation of chorus and hiss: Statistical results from multipoint THEMIS observations. Journal of Geophysical Research: Space Physics, 123. https://doi.org/10.1029/2018JA025725

Allison H. J., Y. Y. Shprits, I. S. Zhelavskaya, D. Wang, A. G. Smirnov, (2021), Gyroresonant wave-particle interactions with chorus waves during extreme depletions of plasma density in the Van Allen radiation belts, Science Advances, 7, doi:10.1126/sciadv.abc0380

Bingham, S. T., Mouikis, C. G., Kistler, L. M., Boyd, A. J., Paulson, K., Farrugia, C. J., et al. (2018). The outer radiation belt response to the storm time development of seed electrons and chorus wave activity during CME and CIR driven storms. Journal of Geophysical Research: Space Physics, 123, 10,139-10,157. https://doi.org/10.1029/2018JA025963.

Bortnik, J.,R. M. Thorne, and N. P. Meredith (2008), The unexpected origin of plasmaspheric hiss from discrete chorus emissions, Nature. 3/6/2008, Vol. 452 Issue 7183, p62-66, DOI:10.1038/nature06741

Bortnik, J., W. Li, R. M. Thorne, V. Angelopoulos, C. Cully, J. Bonnell, O. Le Contel, and A. Roux (2009), An Observation Linking the Origin of Plasmaspheric Hiss to Discrete Chorus Emissions, Science. 2009 May 8, 324(5928):775-8. doi:10.1126/science.1171273.

Bortnik, J., L. Chen, W. Li, R. M. Thorne, and R. B. Horne (2011a), Modeling the evolution of chorus waves into plasmaspheric hiss, J. Geophys. Res., 116, A08221, doi:10.1029/2011JA016499.

Bortnik, J., L. Chen, W. Li, R. M. Thorne, N. P. Meredith, and R. B. Horne (2011b), Modeling the wave power distribution and characteristics of plasmaspheric hiss, J. Geophys. Res., 116, A12209, doi:10.1029/2011JA016862.

Bortnik, J., Chen, L., Li, W., Thorne, R. M., Nishimura, Y., Angelopoulos, V. and Kletzing, C. A. (2016) Relationship between Chorus and Plasmaspheric Hiss Waves in Low-Frequency Waves in Space Plasmas (eds A. Keiling, D.-H. Lee and V. Nakariakov), John Wiley & Sons, Inc, Hoboken, NJ. doi: 10.1002/9781119055006.ch6

Burtis, W. J., and R. A. Helliwell (1969), Banded chorus—A new type of VLF radiation observed in the magnetosphere by OGO 1 and OGO 3, J. Geophys. Res., 74(11), 3002-3010, doi: 10.1029/JA074i011p03002.

Cattell, C. A., Breneman, A. W., Thaller, S. A., Wygant, J. R., Kletzing, C. A., and Kurth, W. S. (2015), Van Allen Probes observations of unusually low frequency whistler mode waves observed in association with moderate magnetic storms: Statistical study, Geophys. Res. Lett., 42, 7273– 7281, doi:10.1002/2015GL065565.

Chen, L., J. Bortnik, R. M. Thorne, R. B. Horne, and V. K. Jordanova (2009), Three-dimensional ray tracing of VLF waves in a magnetospheric environment containing a plasmaspheric plume, Geophys. Res. Lett., 36, L22101, doi: 10.1029/2009GL040451.

Chum, J. and O. Santolík, Propagation of whistler-mode chorus to low altitudes: divergent ray trajectories and ground accessibility, Annales Geophysicae, 23, 3727 - 3738, 2005.

Cornilleau-Wehrlin, N., R. Gendrin, F. Lefeuvre, M. Parrot, R. Grard, D. Jones, A. Bahnsen, E. Ungstrup, and W. Gibbons (1978), VLF electromagnetic waves observed onboard GEOS-1, Space Sci. Rev., 22, 371–382, doi:10.1007/BF00210874.

Darrouzet, F., J. De Keyser, P. M. E. Décréau, F. El Lemdani-Mazouz, and X. Vallières (2008), Statistical analysis of plasmaspheric plumes with Cluster/WHISPER observations, Ann. Geophys., 26(8), 2403-2417.

Gao, Z., Su, Z., Zhu, H., Xiao, F., Zheng, H., Wang, Y., Shen, C., and Wang, S. (2016), Intense low-frequency chorus waves observed by Van Allen Probes: Fine structures and potential effect on radiation belt electrons, Geophys. Res. Lett., 43, 967– 977, doi:10.1002/2016GL067687.

Gao, X., Chen, L., Li, W., Lu, Q., and Wang, S. (2019). Statistical results of the power gap between lower-band and upper-band chorus waves. Geophysical Research Letters, 46, 4098–4105. https://doi.org/10.1029/2019GL082140

Gendrin, R. (1961). Le guidage des whistlers par le champ magnetique. Planetary and Space Science, 5, 274-278. https://doi.org/10.1016/0032-0633(61)90096-4.

Gurnett, D. A., and B. J. O'Brien (1964), High-latitude geophysical studies with satellite Injun 3: 5. Very-low-frequency electromagnetic radiation, J. Geophys. Res., 69(1), 65-89, doi:10.1029/JZ069i001p00065.

Hartley, D. P., Chen, Y., Kletzing, C. A., Denton, M. H. and Kurth, W. S. (2015), Applying the cold plasma dispersion relation to whistler mode chorus waves: EMFISIS wave measurements from the Van Allen Probes. J. Geophys. Res. Space Physics, 120: 1144-1152. doi: 10.1002/2014JA020808.

Hartley, D. P., C. A. Kletzing, W. S. Kurth, S. R. Bounds, T. F. Averkamp, G. B. Hospodarsky, J. R. Wygant, J. W. Bonnell, O. Santolík, and C. E. J. Watt (2016), Using the cold plasma dispersion relation and whistler mode waves to quantify the antenna sheath impedance of the Van Allen Probes EFW instrument, J. Geophys. Res. Space Physics, 121, doi:10.1002/2016JA022501.

Hartley, D. P., C. A. Kletzing, W. S. Kurth, G. B. Hospodarsky, S. R. Bounds, T. F. Averkamp, J. W. Bonnell, O. Santolík, and J. R. Wygant (2017), An improved sheath impedance model for the Van Allen Probes EFW instrument: Effects of the spin axis antenna, J. Geophys. Res. Space Physics, 122, 4420-4429, doi:10.1002/2016JA023597.

Hartley, D. P., Kletzing, C. A., Santolík, O., Chen, L., and Horne, R. B. (2018b). Statistical properties of plasmaspheric hiss from Van Allen Probes observations. Journal of Geophysical Research: Space Physics, 123, 2605-2619. https://doi.org/10.1002/2017JA024593

Hartley, D. P., Kletzing, C. A., Chen, L., Horne, R. B., and Santolik, O. (2019). Van Allen Probes observations of chorus wave vector orientations: Implications for the chorus-to-hiss mechanism. Geophysical Research Letters, 46, 2337-2346. https://doi.org/10.1029/2019GL082111.

Hartley, D. P., I. W. Christopher, C. A. Kletzing, W. S. Kurth, O. Santolík, I. Kolmasova, J. R. Wygant, and J. W. Bonnell (2022), Quantifying the sheath impedance of the electric antennas on the Van Allen Probes, Journal of Geophysical Research: Space Physics (manuscript accepted).

Horne, R. B., Kersten, T., Glauert, S. A., Meredith, N. P., Boscher, D., Sicard-Piet, A., Thorne, R. M., and Li, W. (2013), A new diffusion matrix for whistler mode chorus waves, J. Geophys. Res. Space Physics, 118, 6302– 6318, doi:10.1002/jgra.50594.

Kim, K.-C., and Shprits, Y. (2019). Statistical analysis of hiss waves in plasmaspheric plumes using Van Allen Probe observations. Journal of Geophysical Research: Space Physics, 124, 1904-1915. https://doi.org/10.1029/2018JA026458.

Kletzing, C.A., W.S. Kurth, M. Acuna, R.J. MacDowall, R.B. Torbert, T. Averkamp, D. Bodet, S.R. Bounds, M. Chutter, J. Connerney, D. Crawford, J.S. Dolan, R. Dvorsky, G.B. Hospodarsky, J. Howard, V. Jordanova, R.A. Johnson, D.L. Kirchner, B. Mokrzycki, G. Needell, J. Odom, D. Mark, R. Pfaff Jr., J.R. Phillips, C.W. Piker, S.L. Remington, D. Rowland, O. Santolík, R. Schnurr, D. Sheppard, C.W. Smith, R.M. Thorne, and J. Tyler, The Electric and Magnetic Field Instrument Suite and Integrated Science (EMFISIS) on RBSP, Space Science Reviews, doi:10.1007/s11214-013-9993-6.

Koons, H. C. (1981), The role of hiss in magnetospheric chorus emissions, J. Geophys. Res., 86(A8), 6745–6754, doi:10.1029/JA086iA08p06745.

Koons, H. C., and Roeder, J. L. (1990). A survey of equatorial magnetospheric wave activity between 5 and 8 RE. Planetary Space Science, 38, 1335–1341. https://doi.org/10.1016/0032-0633(90)90136-E

Kurth, W. S., De Pascuale, S., Faden, J. B., Kletzing, C. A., Hospodarsky, G. B., Thaller, S. and Wygant, J. R. (2015), Electron densities inferred from plasma wave spectra obtained by the Waves instrument on Van Allen Probes. J. Geophys. Res. Space Physics, 120: 904-914. doi: 10.1002/2014JA020857.

Lauben, D. S., Inan, U. S., Bell, T. F., and Gurnett, D. A. (2002). Source characteristics of ELF/VLF chorus. Journal of Geophysical Research, 107(A12), 1429. https://doi.org/10.1029/2000JA003019

LeDocq, M. J., D. A. Gurnett, and G. B. Hospodarsky (1998), Chorus source locations from VLF Poynting flux measurements with the Polar spacecraft, Geophys. Res. Lett., 25(21), 4063–4066, doi:10.1029/1998GL900071.

Li, W.,Thorne, R. M., Nishimura, Y., Bortnik, J., Angelopoulos, V., McFadden, J. P., et al. (2010). THEMIS analysis of observed equatorial electron distributions responsible for the chorus excitation. Journal of Geophysical Research, 115, A00F11. https://doi.org/10.1029/ 2009JA014845

Li, W., Thorne, R. M., Bortnik, J., Tao, X., and Angelopoulos, V. (2012), Characteristics of hiss-like and discrete whistler-mode emissions, Geophys. Res. Lett., 39, L18106, doi:10.1029/2012GL053206.

Li, W., D. Mourenas, A. V. Artemyev, O. V. Agapitov, J. Bortnik, J. M. Albert, R. M. Thorne, B. Ni1, C. A. Kletzing, W. S. Kurth and G. B. Hospodarsky (2014), Evidence of stronger pitch angle scattering loss caused by oblique whistler-mode waves as compared with quasi-parallel waves, Geophys. Res. Lett., 41, 6063-6070, doi:10.1002/2014GL061260.

Li, W., L. Chen, J. Bortnik, R. M. Thorne, V. Angelopoulos, C. A. Kletzing, W. S. Kurth, and G. B. Hospodarsky (2015), First evidence for chorus at a large geocentric distance as a source of plasmaspheric hiss: Coordinated THEMIS and Van Allen Probes observation, Geophys. Res. Lett., 42, 241-248, doi: 10.1002/2014GL062832.

Li, W., O. Santolik, J. Bortnik, R. M. Thorne, C. A. Kletzing, W. S. Kurth, and G. B. Hospodarsky (2016), New chorus wave properties near the equator from Van Allen Probes wave observations, Geophys. Res. Lett., 43, 4725-4735, doi:10.1002/2016GL068780.

Li, J., Bortnik, J., An, X. et al. Origin of two-band chorus in the radiation belt of Earth. Nat Commun 10, 4672 (2019). https://doi.org/10.1038/s41467-019-12561-3

Malaspina, D. M., Jaynes, A. N., Boule, C., Bortnik, J., Thaller, S. A., Ergun, R. E., Kletzing, C. A., and Wygant, J. R. (2016), The Distribution of Plasmaspheric Hiss Wave Power with Respect to Plasmapause Location, Geophys. Res. Lett., 43, 7878-7886, doi:10.1002/2016GL069982.

Malaspina, D. M., Jaynes, A. N., Elkington, S., Chan, A., Hospodarsky, G., and Wygant, J. (2021). Testing the organization of lower-band whistler-mode chorus wave properties by plasmapause location. Journal of Geophysical Research: Space Physics, 126, e2020JA028458. https://doi.org/10.1029/2020JA028458.

Mauk, B. H., N. J. Fox, S. G. Kanekal, R. L. Kessel, D. G. Sibeck, and A. Ukhorskiy (2012), Science objectives and rationale for the Radiation Belt Storm Probes mission,Space Sci. Rev.,179, 3-27, doi:10.1007/s11214-012-9908-y.

Meredith, N. P., R. B. Horne, R. M. Thorne, and R. R. Anderson (2003), Favored regions for chorus-driven electron acceleration to relativistic energies in the Earth's outer radiation belt, Geophys. Res. Lett., 30, 1871, doi: 10.1029/2003GL017698, 16.

Meredith, N. P., R. B. Horne, A. Sicard-Piet, D. Boscher, K. H. Yearby, W. Li, and R. M. Thorne (2012), Global model of lower band and upper band chorus from multiple satellite observations, J. Geophys. Res., 117, A10225, doi: 10.1029/2012JA017978.

Meredith, N. P., Horne, R. B., Li, W., Thorne, R. M., and Sicard-Piet, A. (2014), Global model of low-frequency chorus (fLHR < f < 0.1fce) from multiple satellite observations, Geophys. Res. Lett., 41, 280– 286, doi:10.1002/2013GL059050.

Meredith, N. P., Horne, R. B., Shen, X.-C., Li, W., and Bortnik, J. (2020). Global model of whistler mode chorus in the near-equatorial region ($|\lambda_m| < 18°$). Geophysical Research

Letters, 47, e2020GL087311. https://doi.org/10.1029/2020GL087311

Meredith, N. P., Bortnik, J., Horne, R. B., Li, W., and Shen, X.-C. (2021). Statistical investigation of the frequency dependence of the chorus source mechanism of plasmaspheric hiss. Geophysical Research Letters, 48, e2021GL092725. https://doi.org/10.1029/2021GL092725

Omura, Y., Katoh, Y., and Summers, D. (2008). Theory and simulation of the generation of whistler-mode chorus. Journal of Geophysical Research, 113, A04223. https://doi.org/10.1029/2007JA012622

Pope, J. H. (1963), A high-latitude investigation of the natural very-low-frequency electromagnetic radiation known as chorus, J. Geophys. Res., 68, 83–99, doi:10.1029/JZ068i001p00083.

Santolík, O., J. S. Pickett, D. A. Gurnett, and L. R. O. Storey, Magnetic component of narrowband ion cyclotron waves in the auroral zone, J. Geophys. Res., 107(A12), 1444, doi:10.1029/2001JA000146, 2002.

Santolík, O., Gurnett, D. A., Propagation of auroral hiss at high altitudes, Geophys. Res. Lett., 29(10), doi:10.1029/2001GL013666, 2002.

Santolík, O., D. A. Gurnett, J. S. Pickett, M. Parrot, and N. Cornilleau-Wehrlin (2003a), Spatio-temporal structure of storm-time chorus, J. Geophys. Res., 108(A7), 1278, doi:10.1029/2002JA009791.

Santolík, O., M. Parrot, and F. Lefeuvre (2003), Singular value decomposition methods for wave propagation analysis, Radio Sci., 38, 1010, doi:10.1029/2000RS002523, 1.

Santolík, O., J. Chum, M. Parrot, D. A. Gurnett, J. S. Pickett, and N. Cornilleau-Wehrlin, Propagation of whistler mode chorus to low altitudes: Spacecraft observations of structured ELF hiss, J. Geophys. Res., 111, A10208, doi:10.1029/2005JA011462, 2006.

Santolík, O., D. A. Gurnett, J. S. Pickett, J. Chum, and N. Cornilleau-Wehrlin (2009), Oblique propagation of whistler mode waves in the chorus source region, J. Geophys. Res., 114, A00F03, doi:10.1029/2009JA014586.

Santolík, O., J. S. Pickett, D. A. Gurnett, J. D. Menietti, B. T. Tsurutani, and O. Verkhoglyadova (2010), Survey of Poynting flux of whistler mode chorus in the outer zone, J. Geophys. Res., 115, A00F13, doi:10.1029/2009JA014925

Shi, R., Li, W., Ma, Q., Green, A., Kletzing, C. A., Kurth, W. S., et al. (2019). Properties of whistler mode waves in Earth's plasmasphere and plumes. Journal of Geophysical Research: Space Physics, 124, 1035-1051. https://doi.org/10.1029/2018JA026041

Teng, S., Tao, X., and Li, W. (2019). Typical characteristics of whistler mode waves categorized by their spectral properties using Van Allen Probes observations. Geophysical Research Letters, 46, 3607-3614. https://doi.org/10.1029/2019GL082161

Tsurutani, B. T., and Smith, E. J. (1974), Postmidnight chorus: A substorm phenomenon, J. Geophys. Res., 79(1), 118– 127, doi:10.1029/JA079i001p00118.

Usanova, M. E., F. Darrouzet, I. R. Mann, and J. Bortnik (2013), Statistical analysis of EMIC waves in plasmaspheric plumes from Cluster observations, J. Geophys. Res. Space Physics, 118, 4946-4951, doi:10.1002/jgra.50464.

Wang, C., Q. Zong, F. Xiao, Z. Su, Y. Wang, and C. Yue (2011), The relations between magnetospheric chorus and hiss inside and outside the plasmasphere boundary layer:

Cluster observation, J. Geophys. Res., 116, A07221, doi: 10.1029/2010JA016240.

Xiao, F., et al. (2017), Generation of extremely low frequency chorus in Van Allen radiation belts, J. Geophys. Res. Space Physics, 122, 3201-3211, doi:10.1002/2016JA023561.

Zhou, Q., F. Xiao, C. Yang, S. Liu, Y. He, J. R. Wygant, D. N. Baker, H. E. Spence, G. D. Reeves, and H. O. Funsten (2016), Evolution of chorus emissions into plasmaspheric hiss observed by Van Allen Probes, J. Geophys. Res. Space Physics, 121, 4518-4529, doi: 10.1002/2016JA022366.

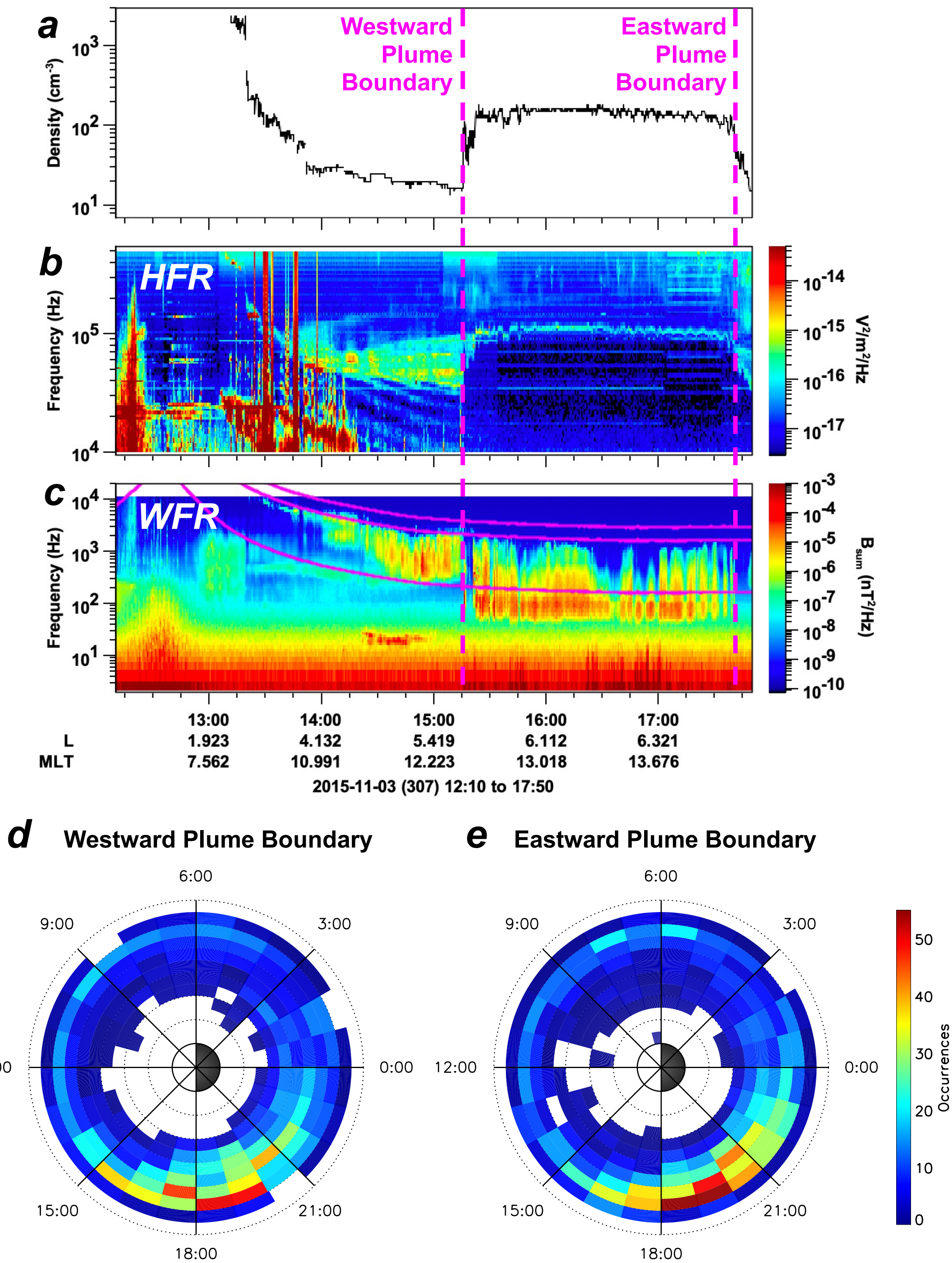

Figure 1. The (a) plasma density, (b) HFR electric field observations, and (c) WFR magnetic field observations by Van Allen Probe B during the passage of a plasmaspheric plume with $0.05 f_{ce}$, $0.50 f_{ce}$, and $0.90 f_{ce}$ shown in magenta. Location in MLT and L of

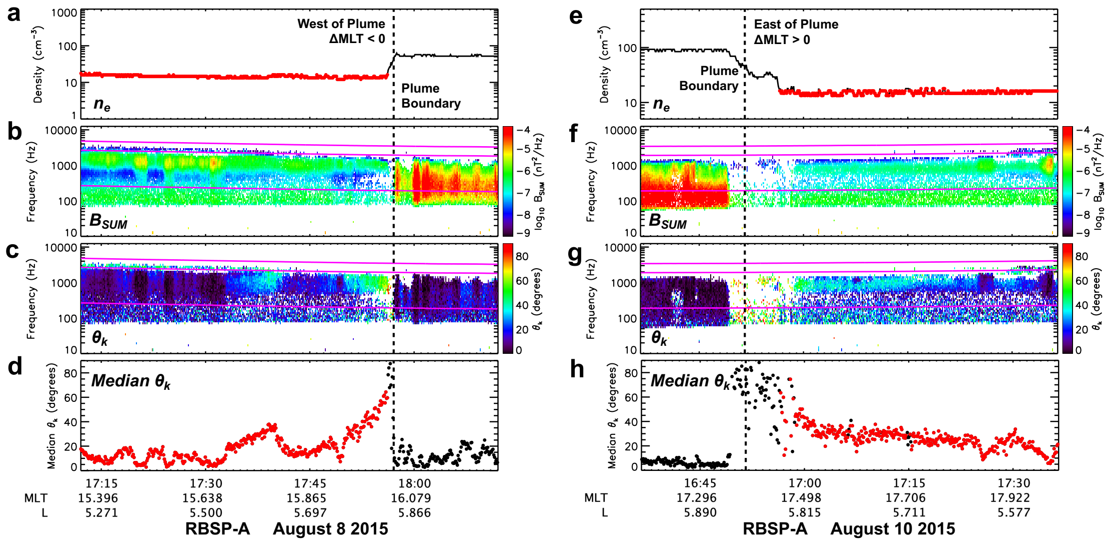

Figure 2. Two case study events of chorus near plumes showing (a and e) the plasma density, (b and f) magnetic field wave power, (c and g) wave normal angle, θ_k, and (d and h) median θ_k between 0.05 and 0.50 f$_{ce}$. Red data indicate time periods used in the analysis.

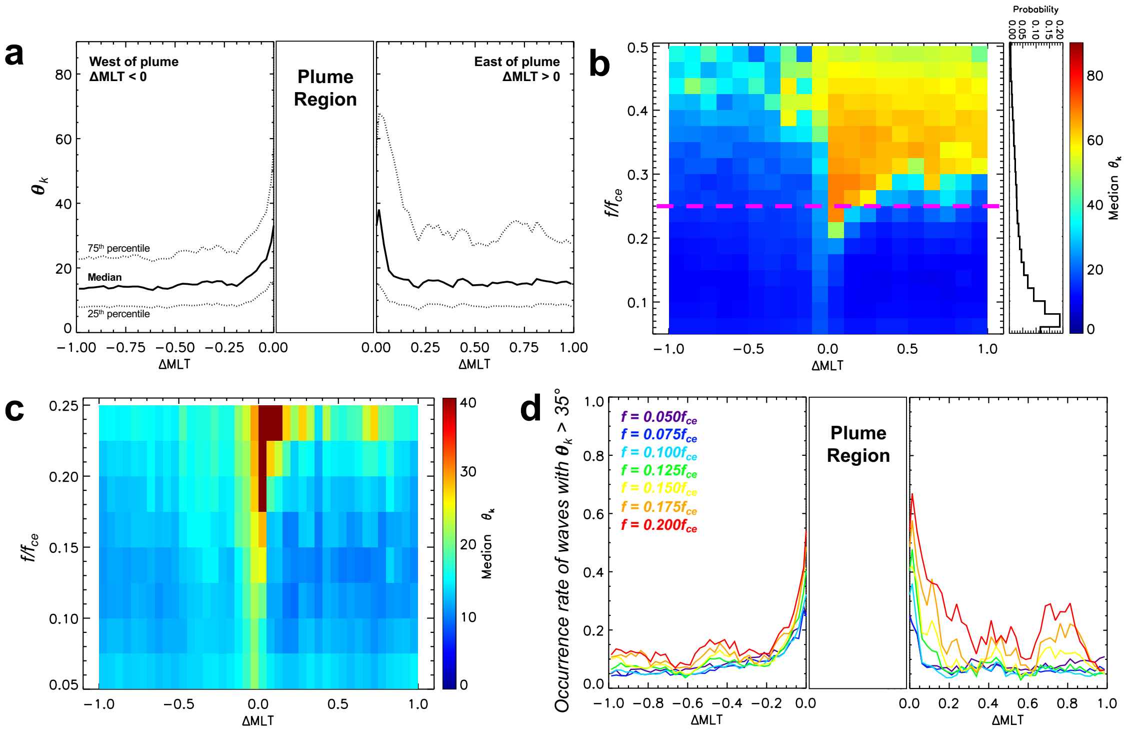

Figure 3. (a) the median wave normal angle as a function of distance from the plume boundary in MLT. (b and c) the median wave normal angle as a function of distance from the plume in MLT and wave frequency, magenta line indicates 0.25 f/f_{ce}, probability distribution as a function of wave frequency is also shown. (d) the occurrence rate of chorus waves with $\theta_k > 35°$ as a function of distance from the plume.

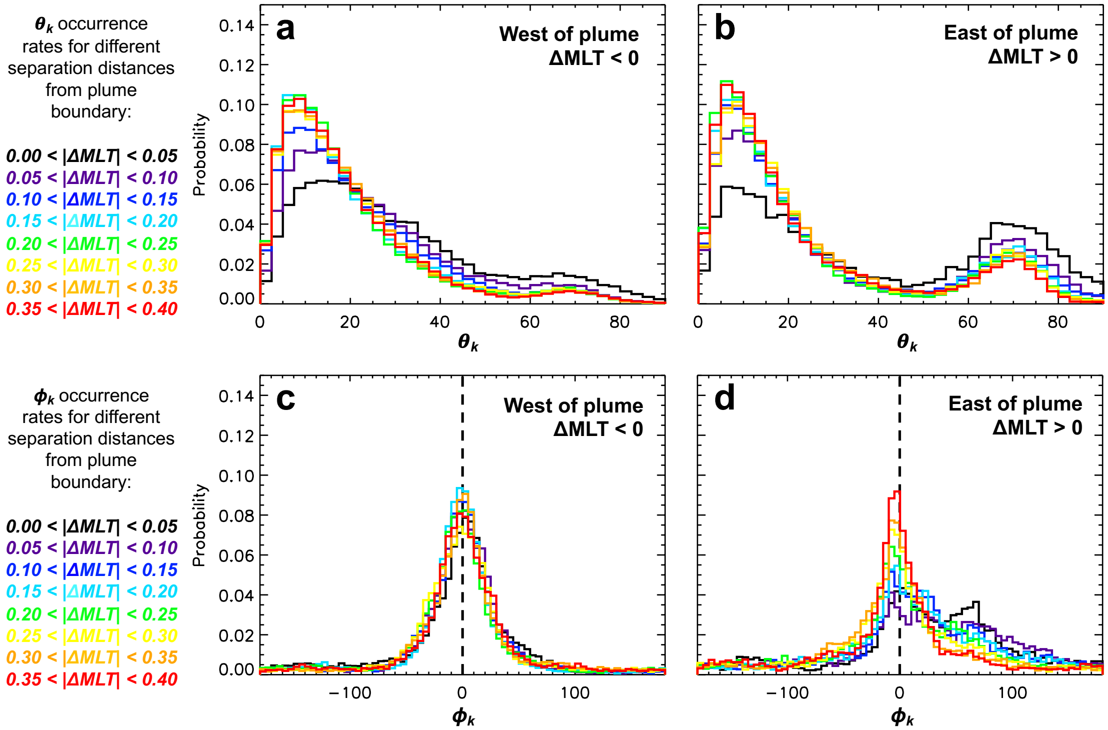

Figure 4. PDFs of the (a and b) polar wave vector angle, and (c and d) azimuthal wave vector angle for different separation distances from the (left) West and (right) East plume boundary.